2024 IEEE 63rd Conference on Decision and Control (CDC)
December 16-19, 2024. MiCo, Milan, Italy

Comparison of closed loop control strategies for the activation of genetic switches

Alexander P.S. Darlington[1], Ahmad A. Mannan[2] and Declan G. Bates[1]

***Abstract*— The performance of biomanufacturing systems can be improved by incorporating inducible synthetic gene circuits which 'switch' the microbial cell factories from growth to production upon the manual addition of a small molecule activator. Here, we consider feedback strategies which enable autonomous activation of a genetic circuit based on cell state. Using a multi-scale modelling framework which takes into account the dynamics of microbial growth and pathway production, we show that population-based feedback offers a promising strategy for autonomous activation of genetic switches.**

I. INTRODUCTION

Microorganisms can be engineered to produce a variety of chemicals, from drug precursors to food colours. However, currently, engineered microbial "cell factories" show limited efficiency as chemical production often results in poor cell growth due to the cell's inherent constraints in its cellular economy. Expression of many engineered pathways drains host cell metabolism, creating a hard growth-synthesis trade-off. Though higher synthesis means higher product yield, the cost to growth fundamentally limits the achievable volumetric productivity, and so too the economic viability of bioproduction. A promising strategy for decoupling the growth-synthesis trade-off is to engineer a two-stage production processes; where cells grow first, before production from the larger population is activated (reviewed in [1],[2]). These strategies can be implemented in living cells using gene circuits (module Q in Fig. 1a) which activate the pathway (A module) and inhibit host processes (E in Fig. 1a). Upon activation, the circuit deactivates growth processes and simultaneously activates synthesis. A number of such "two-sided" circuits, which regulate both E and A, have been engineered in living cells [3]. We recently proposed a simplified "one-sided" topology, containing only one regulatory loop which acts to inhibit growth through E [4]. We showed that the cell's endogenous constraints enable this topology to facilitate near optimal performance. As growth is inhibited, the cell shifts to an 'enzyme dominated' proteome which activates the pathway module in the absence of 'direct' activation.

However, to date, most growth/production circuits rely on exogenous activation of this switch by the addition of small molecule inducers to the culture medium at some given time point. Such chemical inducers are often expensive which can dramatically increase the costs of a given bioprocess. Whilst there is increasing interest in the use of cheaper alternatives, these alternatives are often metabolic by-products and so enter the cell's metabolism reducing their concentration over time. We recently showed that engineering bistable gene circuits offers a potential means to reduce the concentration of expensive inducers [5].

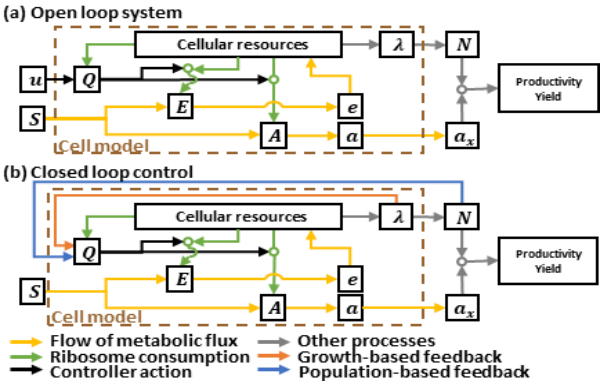

Fig. 1. Block diagram of the controllers and depicting host-pathway interactions. Blocks represent gene/protein modules composed of transcription and translation reactions. Consumption of cellular resources are shown as green arrows. Metabolic fluxes are shown as yellow arrows. Other mass or information flow is shown as grey arrows. The blocks represent the following: S, the substrate pool; E, the host metabolism; e, the translational precursors; A, the synthetic metabolic pathway; a, the intracellular product; a_x, the extracellular product; Cellular resources, the pool of ribosomes and amino acids which are consumed by translation; λ, the cells growth rate; N, the cell population. The growth-product switch is controlled by the Q module. (a) In the open loop system, Q is activated by an input u. (b) In the closed loop systems, Q is activated by either cell growth rate λ or population size N.

In this paper, we consider an alternative strategy; the creation of autonomous systems where the system "self switches" without the need for manual measurement and cutting out inducer costs altogether (blue, orange lines in Fig. 1b). Some such switches have been engineered in living cells (e.g. [6], further reviewed in [7]) but to date the design of such systems within host constraints has not been rigorously considered. In Section II, we develop a multi-scale model of the host physiology, pathway dynamics and gene circuit controller. This model captures key host-circuit interactions which can complicate synthetic circuit design [8]. In Section III, we use phenomenological models of biological processes which could close the feedback loop to evaluate potential strategies which may enable autonomous control in the absence of external input. In Section IV, we use multi-objective optimisation to design controllers which maximise key industrial performance metrics from batch

APSD acknowledges funding from Royal Academy of Engineering under their Research Fellowship scheme. [1]Warwick Integrative Synthetic Biology Centre, School of Engineering, University of Warwick, Coventry, UK. [2]Department of Bioengineering, Imperial College London, London, UK. For the purpose of open access, the authors have applied a Creative Commons Attribution (CC BY) license to any Author Accepted Manuscript version arising. (correspondence to a.darlington.1@warwick.ac.uk)

cultures: volumetric productivity (total product synthesis rate) and yield (substrate-to-product conversion ratio). We show that population-based feedback performs as well as optimal open loop inducible systems. In Section V, we explore how design rules change when the controller circuit topology is simplified as we proposed in [4]. In Section VI, we compare the dynamics of the different control systems to identify the basis of the difference in performance. In Section **??**, we develop a realistic model of how population-based control can be implemented in living cells and show that the additional resource consumption caused by the population-sensing system reduces the performance of the simple "one-sided circuit".

II. Context-based model of the open loop switch

We use a multi-scale modelling framework which captures microbial cell metabolism, gene expression and growth [9]. This non-linear 'self-replicator' model of host and pathway is composed of 26 coupled ordinary differential equations which capture the time evolution of a simple metabolism (consisting of a substrate s_i, universal energy carrier e and product a_i), gene expression of a coarse-grained proteome (consisting of transporters p_T, metabolic enzymes p_E, host proteins p_H, ribosomal proteins p_R, pathway enzymes p_A and regulator protein p_Q), and cell growth.

A. The gene expression model

Protein production is considered as a two step process composed of transcription and translation. The mRNAs of gene Y (m_Y) are born spontaneously at a rate proportional to the cell's energy (e) and any regulator protein ($p_{Y'}$). The mRNA (reversibly) binds to free ribosomes (R) to produce translation complexes (c_Y). These undergo translation (protein birth) at rate $T_L(c_Y,\ e)$ to produce proteins (p_Y). All species dilute due to growth (λ) and mRNAs are also subject to decay (δ_m). Applying the law of mass action to this scheme gives the following dynamics:

$$\dot{m}_Y = T_X(e, p_{Y'}) - b_Y \cdot R \cdot m_Y + u_Y \cdot c_Y - (\lambda + \delta_m) \cdot m_Y \quad (1)$$

$$\dot{c}_Y = b_Y \cdot R \cdot m_Y - u_Y \cdot c_Y - T_L(c_Y,\ e) - \lambda \cdot c_Y \quad (2)$$

$$\dot{p}_Y = T_L(c_Y,\ e) - \lambda \cdot p_Y \quad (3)$$

The translation rate $T_L(c_Y,\ e)$ is:

$$T_L(c_Y,\ e) = (1/n_Y) \cdot c_Y \cdot (\gamma_{max} \cdot e)/(\kappa_\gamma + e) \quad (4)$$

where $(\gamma_{max} \cdot e)/(\kappa_\gamma + e)$ is a Michaelis-Menton equation which scales the maximal peptide elongation rate (γ_{max}) by the cell's internal energy supply (e) and a constant of κ_γ. n_Y is the length of the protein in amino acids, see [9] for a complete discussion. The transcription rate $T_X(e,\ p_{Y'})$ is given by the Michaelis-Menton equation:

$$T_X(e,\ p_{Y'}) = \Big(\omega_0 + \omega_Y \cdot \Psi_Y(p_{Y'})\Big) \cdot \left(\frac{e}{\theta_Y + e}\right) \quad (5)$$

where ω_0 is a constant basal expression (set to 10^{-3} throughout) and ω_Y is the maximal mRNA birth rate. $\Psi_Y(p_{Y'})$ is the regulation of m_Y birth by the protein $p_{Y'}$. The $e/(\theta_Y + e)$ expression scales the birth rate by the cell's internal energy. In the core model without any engineered regulation:

$$\Psi_Y(\cdot) = \begin{cases} 1 & Y = \{T, E, A, r, R\} \\ \left(1 + \left(\frac{p_H}{K_H}\right)^{h_H}\right)^{-1} & Y = \{H\} \end{cases} \quad (6)$$

We model ribosome biogenesis as a multistep process composed of r-protein (p_R) and rRNA (r) production and assembly into the function ribosome (with full dynamics described in [9]). Therefore the dynamics of the free ribosome pool are:

$$\dot{R} = b_\rho \cdot p_R \cdot r - u_\rho \cdot R - \lambda \cdot R ... \\ ... + \sum_X \Big(T_L(c_X,\ e) - b_X \cdot m_X \cdot R + u_X \cdot c_X\Big) \quad (7)$$

where p_R and r are r-rpoteins and rRNAs repectively which form the functional free ribosome and $X = \{T,\ E,\ H,\ R,\ A,\ Q\}$. All genes within the model are connected to this single pool by ribosome-mRNA association reactions through the $\sum_X(\cdot)$ term. As one gene Y increases the $R \rightarrow c_Y$ rate increases which perturbs the other genes in the set X through the $\sum_X(\cdot)$ term.

B. The pathway and cell metabolic models

The metabolic model is composed of an extracellular substrate (S) which is imported into the cell at rate v_{uptake} by transporters (p_T) to form a pool of internalised substrate (s_i). This is utilised for host processes at rate v_{host} (e.g. energy/amino production, lumped together into an anabolic driver species e) or the engineered pathway at rate v_{prod}. Applying the Law of Mass Action to determine the dynamics of the s_i concentrations gives:

$$\dot{s}_i = v_{uptake}(S, p_T) - v_{host}(s_i, p_E) - v_{prod}(s_i, p_A) - \lambda \cdot S_i \quad (8)$$

The e is consumed by translation and has dynamics:

$$\dot{e} = n \cdot v_{host}(s_i, p_E) - \sum_Y \Big(n_Y \cdot T_L(c_Y,\ e)\Big) - \lambda \cdot e \quad (9)$$

where n is the number of e molecules produced from each s_i molecule. The dynamics of intracellular product concentration (a_i) are:

$$\dot{a}_i = v_{prod}(s_i,\ p_A) - \lambda \cdot a_i \quad (10)$$

The rates of these reactions are modelled with Michaelis-Menten kinetics $v_{rxn}(x, p_Y) = \big(v_Y \cdot x \cdot p_Y\big)/\big(\kappa_Y + x\big)$, where x is the substrate concentration and p_Y is the concentration of the catalysing enzyme with a turnover number of v_Y and Michaelis constant of κ_Y. We denote host transport proteins T (i.e. $Y = T$), host enzymes as E and the enzyme of the engineered bioprocess to be A.

C. The open loop controller

The concentration, and ratio between, p_E and p_A determines the systems performance; high p_E, low p_A favours growth at a loss of product and *vice versa*. To dynamically control the birth rate of p_E and p_A, we introduce a regulator protein p_Q which activates m_A production and inhibits m_E

production. To model this regulation we update Ψ_E and Ψ_A to:

$$\Psi_E(p_Q) = \frac{{K_E}^{n_E}}{{K_E}^{n_E} + {p_Q}^{n_E}} \quad \Psi_A(p_Q) \quad = \frac{{p_Q}^{n_A}}{{K_A}^{n_A} + {p_Q}^{n_A}} \quad (11)$$

We introduce it's mRNA (m_Q) and translation complex (c_Q) and modify Eq. 7 Eq. 9, and Eq. 15 to take account of the additional R and e consumption and the impacts on growth. The dynamics of the regulator follow those in Eq. 1-3. The transcription rate $T_X(e,U)$ for the controller system is

$$T_X(e,U) = \Big(\omega_0 + \omega_Q \cdot U\Big) \cdot \Big(\frac{e}{\theta_Q + e}\Big). \quad (12)$$

For the open loop system:

$$U = u_0. \quad (13)$$

Dynamic control can be created with a step input at time t_{ind}:

$$U = \begin{cases} 0 & t < t_{ind} \\ u_0 & t \geq t_{ind} \end{cases} \quad (14)$$

D. The batch culture model

We derive the cell growth rate as a consequence of total production rate (see [9] for derivation):

$$\lambda = (1/M_0) \cdot \Big((\gamma_{max} \cdot e)/(\kappa_\gamma + e)\Big) \cdot \sum_X \Big(c_X \Big) \quad (15)$$

The three state culture model is composed of: the cell population (N), the external substrate (S, which is taken up by cells), the extracellular product (A) which is exported from the cell. The dynamics of this system are:

$$\dot{N} = \lambda(\cdot) \cdot N \quad \dot{S} \quad = -v_{uptake}(\cdot) \cdot N \quad \dot{A} = v_{prod}(\cdot) \cdot N \quad (16)$$

E. Biotechnological performance metrics

To characterise any specific controller design (i.e. controller topology and parameterisation thereof), the system of equations is simulated until all substrate is depleted ($S(t) = 0$), a time point we define as t_{end}, and we calculate the yield (J_y) and the volumetric productivity (J_{vp}) as follows:

$$J_y = A(t_{end})/S(0) \quad \text{and} \quad J_{vp} = A(t_{end})/t_{end}. \quad (17)$$

These metrics are key to designing real world bioprocesses, with volumetric productivity being a key driver of production times, and therefore economic viability of a given process, and yield being the determinant of bioprocess efficiency.

III. Closed loop system performance

The closed loop control strategies in Figure 1b were implemented phenomenologically by updating the function $U(\cdot)$. Growth-based feedback, where growth inhibits the circuit, is modelled by:

$$U = 1/(1 + (\lambda/K_\lambda)) \quad (18)$$

where K_λ controls the strength of the feedback: as $K_\lambda \to 0$, $U \to 0$, as $K_\lambda \to \text{inf}$, $U \to 1$. Population-based feedback, where the circuit is activated by the total cell population, is:

$$U = (N/K_N)/(1 + (N/K_N)) \quad (19)$$

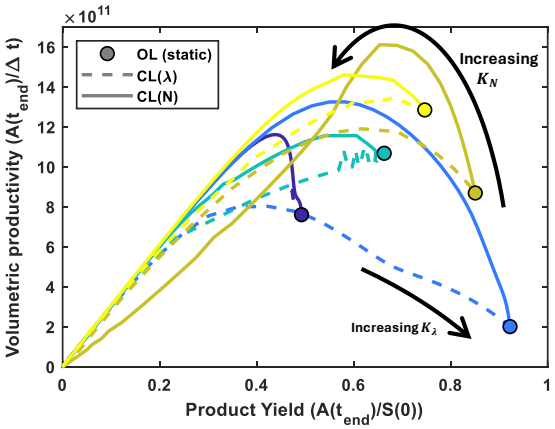

Fig. 2. Closed loop control increases volumetric productivity. A selection of designs were simulated (circles)

where N is the population and K_N controls the strength of the controller activation. Over the course of growth, population size increases: when $N < K_N$, $U < 0.5$ and when $N > K_N$, $U > 0.5$ therefore K_N determines the point at which the controller is activated. We initially explored the impact of these strategies on a set of designs drawn from across the design space. For increasingly stronger growth-based feedback (decreasing K_λ), volumetric productivity increases at a cost of yield until a peak in performance at which point both metrics fall (Fig. 2, dotted lines). Population-based feedback can significantly increase volumetric productivity at only a minor loss of yield (Fig. 2, solid lines). Increasing K_N increases volumetric productivity to a maximum before both metrics fall.

IV. Population-based feedback outperforms growth rate-based control

To compare optimal performance of the different systems, and identify any trade-off between the two objectives of volumetric productivity and yield, we employed a multi-objective optimisation routine (see Appendix for description of numerical methods) to evaluate a number of control strategies across any potential trade-off. We compared the following strategies:

- Strategy 1. An open loop static approach where U takes the form as in Eq. 13
- Strategy 2. An open loop dynamic approach where U takes the form of a step response as in Eq. 14
- Strategy 3. Growth-based feedback where U takes the form in Eq. 18
- Strategy 4. Population-based feedback where U takes the form in Eq. 19

For each controller topology, we optimised the parameter set (K_{opt}) related to (i) the expression and action of the genetic switch (the transcription rates, i.e. $\omega_E, \omega_A, \omega_Q$, and dissociation constants of the controlling transcription factor i.e. K_E and K_A) and (ii) the parameters governing the controller (for Strategy 2, t_{ind}, for Strategy 3, K_λ, and for Strategy 4, K_N). Given that the volumetric productivity and yield objectives vary over orders of magnitude we use the same multi-step optimisation approach we have presented

previously [4]. Firstly, we use a genetic algorithm to solve two optimisation problems to maximise J_y and J_{vp} (and yielding $J_{y,max}$ and $J_{vp,max}$, respectively). To identify the Pareto optimal designs and any performance trade-off between these two extremes, we used a multi-objective genetic algorithm to solve the following optimisation problem:

$$\begin{aligned} &\underset{K_{opt}}{\text{maximise}} \quad \left(J_y/J_{y,max},\ J_{vp}/J_{vp,max}\right) \\ &\text{subject to} \quad lb \leq K_{opt} \leq ub. \end{aligned} \tag{20}$$

All four strategies show a trade-off between volumetric productivity and yield; increasing one objective necessitates a decrease in the other (Fig. 3a). The λ-based controller does *not* outperform static open loop approaches – i.e. the Pareto fronts for strategies 1 and 3 overlap (Fig. 3a). Analysis of the designs along the Pareto fronts show the approaches have similar parametric characteristics with high ω_E values, low ω_A. For both strategies, Q-regulation strength should be weaker on the ω_E (i.e. higher K_E the dissociation constant) and stronger on ω_A (Fig. 3b). The Pareto fronts suggest that production and regulation of p_E through ω_E and K_E is key in determining the position along the volumetric productivity/yield trade-off, with lower expression or tight binding favouring higher yield. K_λ, i.e. the strength of the growth based feedback, is constant across the trade-off which is why this closed-loop strategy gives the same performance as the static open-loop strategy. Dynamic control (Strategy 2) facilitates a near doubling of volumetric productivity (compare to the static open loop approach) and our optimisation shows that the N-based controller (Strategy 3) achieves a further slight increase (Fig. 3a, dark blue curve). The Pareto optimal designs for Strategy 2 and 3 differ both quantitatively and qualitatively suggesting the two strategies do not share design rules (Fig. 3b). In Strategy 2, ω_E and ω_A are of similar order of magnitude with lower K_E (tighter binding) and higher K_A (weaker binding). The production of Q, through ω_Q is low and constant across the trade-off. t_{ind} is the key determinant of the volumetric productivity/yield trade-off with shorter t_{ind} (i.e. earlier induction times) increasing yield at a loss of productivity. Whilst a similar qualitative and quantitative trend in K_E and K_A is seen in Strategy 3, the transcription rates show quantitative differences. In the population-based feedback system, ω_Q is 10 times higher than in the dynamic control strategy. In Strategy 3, ω_E is two orders of magnitude lower than ω_A and in comparison to the dynamic control ω_E should be an order of magnitude lower while ω_A needs to be over one order of magnitude higher. K_N is the key determinant of the trade-off between volumetric productivity and yield.

V. Redesign of Simplified Switches for Closed Loop Control

In [4], we proposed a simplified genetic switch design which relies only on inhibition of growth (i.e. $\Psi_E(p_Q)$ while $\Psi_A = 1$) rather than inhibition of growth *and* activation of the pathway ($\Psi_E(p_Q)$ *and* $\Psi_A(p_Q)$). Having showed that population-based feedback can achieve the same performance as induction, we repeated our analysis with these

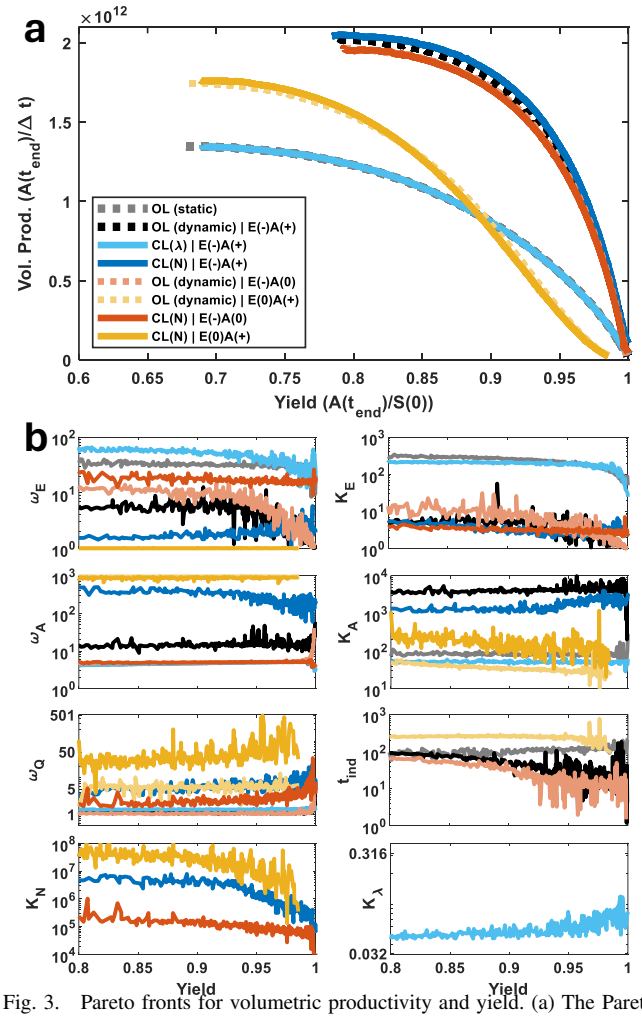

Fig. 3. Pareto fronts for volumetric productivity and yield. (a) The Pareto fronts were identified by the optimisation routine described in Section IV. OL (static) corresponds to constant input U, OL (dynamic) corresponds to a step input for U. CL (λ) corresponds to growth-based controller where U takes the form in Eq. 18. CL(N) corresponds to the population-based controller where U takes the form in Eq. 19. E(-)A(+) corresponds to "dual control" systems where E is inhibited by Q and A is activated by Q. E(-)A(0) corresponds to a "one-sided" control system where Q only regulates E. E(0)A(+) corresponds to a "one-sided" control system where Q only regulates A. (b) Pareto-front designs identified by solving the multi-objective optimisation problem. Line colours correspond to those in (a).

simpler gene circuits. We tested the following topologies:

$$\Psi_E = f(p_Q) \quad \Psi_A = g(p_Q) \quad \text{[E(-1)A(+1)]} \tag{21}$$
$$\Psi_E = f(p_Q) \quad \Psi_A = 1 \quad \text{[E(-1)A(0)]} \tag{22}$$
$$\Psi_E = 1 \quad \Psi_A = g(p_Q) \quad \text{[E(0)A(+1)]} \tag{23}$$

where $f(p_Q)$ takes the form of Ψ_E and $g(p_Q)$ takes the form of Ψ_A in Eq. 11. We re-solved the optimisation problem in Eq. 20 for each circuit topology considering both the open loop dynamic approach (where U is a step input) and population feedback (where U is proportional to N as in Eq. 19). As previously observed, the "one-sided" controller, E(-)A(0), performs nearly as well as the original "dual control" system (e.g. E(-)A(+)). We find that population-based feedback enables the same performance to be achieved, when compared to that produced with dynamic induction (Fig. 3a). Whilst in Section IV, we observed that autonomous controllers for the "dual control" system showed significant

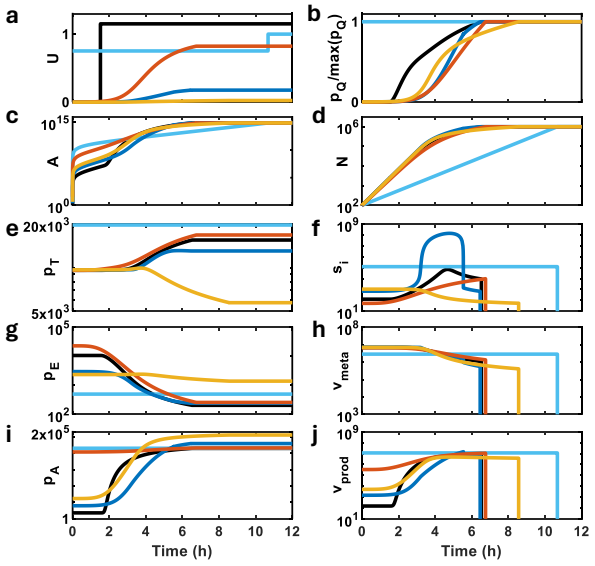

Fig. 4. Dynamics of the designs with high volumetric productivity and yield. Designs from Fig. 3a with yields of 0.85 were simulated and the internal dynamics of the model shown. The strategy is shown by the colour of the line as in Fig. 3a. (a) The input signal (U). (b) The normalised concentration of the controlling transcription factor (p_Q). (c) The extracellular product (A). (d) The population size (N). (e) The transporter protein per cell (p_T). (f) The internalised substrate (s_i). (g) Host enzyme per cell (p_E). (h) Flux from $s_i \rightarrow e$. (i) Pathway enzyme per cell (p_A). (j) Flux from $s_i \rightarrow a_i$.

changes in parameters for the inducible system, we do not see such differences for the two "one-sided" topologies (Fig. 3b) – i.e. there is large overlap between the light (inducible) and dark (autonomous) lines for the "one-sided" systems. This suggests that such systems could be made autonomous with only minimal redesign.

For the E(-1)A(0) topology, the optimal values for the inducible and autonomous systems are similar with only minor increases in ω_E and decreases in K_E required. Therefore, when producing an autonomous system, the optimal designs favour stronger transcription but a stronger regulation of that higher production rate. We observe a general increase in ω_Q in the autonomous system when compared to the inducible system and find that across the front ω_Q increases with increasing yield. This represents a different approach to design: in the inducible system, p_Q activation is constant with the strength of the regulation varying along the front; in the autonomous system the regulation strength is constant with the induction a key driver in performance. As with the "two-sided" system, increasing yield is associated with decreased K_N (equivalent to earlier activation). For the E(0)A(+1) system, the optimal performance is much worse than the two topologies which regulate the host metabolism. Whilst the optimisation routine has identified the bound for the ω_E and ω_A transcription rates these correspond to the biologically feasible values [10].

VI. Population-based feedback creates an autonomous growth-production switch

To determine the reasons for the different performance of the four strategies in Section IV, we compared the time evolution of select species and rates, for designs with the same yield (here 0.85) for Strategies 2, 3 and 4. We also consider the two "one-sided" controllers proposed in V. That is controllers corresponding to the black and blue curves from Fig. 4 and the orange and yellow curves from Fig. 4.

Strategy 3 (λ-based feedback, light blue) does not create a dynamic input signal; rather the control is applied constantly in the same way as Strategy 1 (Fig. 4a) until substrate depletion. The dynamics of Strategy 1 (constant input, not shown) and 3 are the same across all key bioprocesses. This constant input results in a constant (low) growth rate (Fig. 4d) and constant v_{prod}, which only falls when extracellular substrate S falls to zero (Fig. 4j). The system shows no response to the changes in λ before extracellular substrate S depletion – there is no dynamic growth to production switch.

Both Strategy 2 (open loop dynamic induction, black curves) and 4 (population-based feedback, dark blue curves) show a biphasic production. There is an initial growth phase with low A production (see low rate of A accumulation in Fig. 4c). At some time, the rate of A production increases and growth rate falls (Fig. 4d) – this can be observed by the increasing gradient of A accumulation in Fig. 4c). The population-based feedback system shows a longer and lower activation (i.e. U shows a longer rise time and lower maximum) and includes a not insignificant basal level of production (Fig. 4a, d). This results in a prolonged growth phase (Fig. 4d) and higher population when the population begins to switch to the production phase. As the switch activates, p_E falls (Fig. 4g), enabling the intracellular substrate s_i to accumulate (Fig. 4f). This increase in substrate supply for p_A, in comparison to Strategy 2, enables a short lived increase in v_{prod} (Fig. 4j).

The two "one-sided" gene circuits show a weaker biphasic growth/production - with much smaller increases in v_{prod} over the timecourse (Fig. 4j). The E(0)A(+) topology activates earlier than the dual controller but this activation is slow. The production of p_A dominates the dynamics, with others changing relatively little. The system has a higher v_{prod} and therefore shows extended culture times which limits volumetric productivity (Fig. 4c, inset). The E(-)A(0) system activates more slowly than the dual control system; the constitutive production of p_A exerts a burden during growth which enhances v_{prod} but also reduces λ. This results in the circuit activating at lower population size and limits productivity – although the increase in s_i after the switch due to non-regulatory interactions which increase p_T results in only a little lengthening of the total culture time (Fig. 4e).

These dynamics are replicated across most of the Pareto front (Fig. 5). Across the front, the population-based feedback system responds more slowly than the optimal dynamic system (Fig. 5a). For systems with higher volumetric productivity, the system rapidly reaches its maximum activation. As yield increases, the system activates earlier (i.e. decrease in K_N leads to decreased in time when the system reaches 10% activation). As yield increases, the time between the 10% and 90% activation times increases. The highest yielding designs are activated earlier (with low K_N) and have smaller differences in population between the 10%, 50% and 90%

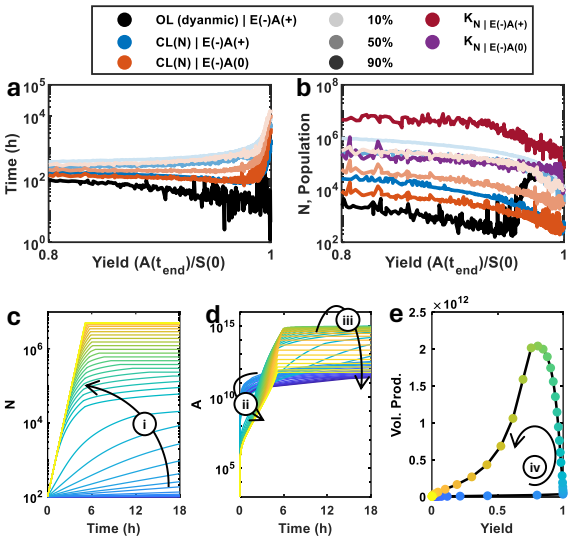

Fig. 5. Impact of K_N on the system dynamics. Panels (a) and (b) are based on the Pareto optimal solutions in Fig. 3. Panels (c-e) are based on the optimal design of the "two-sided" switch whose dynamics are shown in Fig. 4. (a) Time of activation in population-based feedback systems in comparison to the open loop dynamic induction system. Designs are selected from across the Pareto optimal solutions. The black line shows the t_{ind} values for Strategy 2. The coloured lines correspond to percentage of system activation. (b) Population size at the point of activation in the population-based feedback system in comparison to the open loop dynamic induction system. The optimal K_N values from across the Pareto optimal solutions are shown in red and purple. (c) Population size over time. (d) Extracellular A over time. (e) Yield versus volumetric productivity trade-off for the designs in (c) and (d). Selected points are highlighted.

activation states due to lower growth rate. This shows high yielding designs are achieved by those with low growth and high production (similar to early activation of the growth production switch in Strategy 2). These design rules hold for the "one-sided" system where the host enzyme (E) is regulated but we see a general earlier activation at smaller population sizes which is the key cause of limited volumetric productivity.

For a given design, low values of K_N lead to high production (Fig. 5d) and low population ((Fig. 5c) - resulting in poor yield and low productivity (Fig. 5e). As K_N increases, the controller acts to delay production (arrow ii in Fig. 5d), enabling increased population growth (arrow i in Fig. 5c). This enables increased volumetric productivity (arrow iv in Fig. 5e). After the peak in productivity, increasing K_N results in decreased total production (arrow iii in Fig. 5d) which limits yield.

VII. CONCLUSIONS

Here, we compared by simulation and optimization, two potential strategies for engineering autonomous (or 'cell controlled') activation of genetic switches. We showed that population-based feedback outperforms growth-based control and that such a system creates an autonomous growth-production switch system. We showed that such feedback can achieve the same performance as induction by extracellular molecules and is therefore a promising strategy making biomanufacturing genetic switches autonomous without the need for human or computer-based control.

APPENDIX

The model was implemented in MATLAB 2023a with dynamics simulated with the in-built stiff solver *ode15s* with absolute and relative tolerances of 10^{-6} and setting the *NonNegative* flag such that no states could be less than zero. To achieve specific designs (i.e. design parametrisations), we use the *ga* and *gamultiobj* functions from MATLAB's Global Optimisation Toolbox (version 23.2), together with the Parallel Computing Toolbox (version 23.2). Initial conditions for the multiscale simulation were determined by simulating the cell and process model (i.e. $\dot{N} = \dot{S} = \dot{A}$) to steady state from the following initial conditions $N = 0$, $S = 10^4$, $s_i = 10^2$, $e = 10^2$, $p_T = p_E = R = 100$. The steady state concentrations were then used as initial conditions for cell and process species in the multiscale models. The simulations of the multiscale model species were initialised at $N = 10^3$, $S = 1 \times 10^{15}$. We simulated the model across a period of 28 days. The host model parameters are $\phi_e = 0.5$, $v_T = 728$ min^{-1}, $v_E = 5800$ min^{-1}, $\kappa_E = \kappa_T = 1000$ molecules, $\omega_T = \omega_E = 4.14$ mRNAs $\cdot$ min^{-1}, $\omega_H = 948.93$ mRNAs $\cdot$ min^{-1}, $\omega_r = 3170$ mRNAs $\cdot$ min^{-1}, $\omega_R = 930$ mRNAs $\cdot$ min^{-1}, $\pi_T = \pi_E = 4.38$ molecules, $\pi_R = 426.87$ molecules, $n_T = n_E = n_H = 300$ amino acids, $n_R = 7459$ amino acids, $b_T = b_E = b_H = b_R = 1$, $u_T = u_E = u_H = u_R = 1$, $b_\rho = 1$, $u_\rho = 1$, $\delta_m = 0.1$ min^{-1}, $\kappa_H = 121775$ molecules, $h_H = 8$, $\gamma_{max} = 1260$ amino acids per min, $\gamma_\kappa = 7$ molecules, $M_0 = 10^8$ amino acids. The circuit and pathway parameters (where $X = \{A, Q\}$) are $w_0 = 10^{-3}$, $\omega_X = 20$ mRNAs $\cdot$ min^{-1}, $\pi_X = 4.38$ molecules, $n_X = 300$ amino acids, $b_X = 1$, $u_X = 1$, $v_A = 580$ min^{-1}, $\kappa_A = 1000$ molecules. $V_{cell} = 10^{-15}$ L, $V_{cult} = 1$ L, $k_f = 1 \times 10^2$ molecules$^{-2} \cdot$ min^{-1}, $k_r = 10^-6$ min^{-1}.

REFERENCES

[1] C. J. Hartline, A. C. Schmitz, Y. Han, and F. Zhang, "Dynamic control in metabolic engineering: Theories, tools, and applications," *Metabolic Engineering*, 2020.

[2] D. Banerjee and A. Mukhopadhyay, "Perspectives in growth production trade-off in microbial bioproduction," *RSC Sustainability*, vol. 1, pp. 224–233, 2023.

[3] M. Ream and K. L. J. Prather, "Engineered autonomous dynamic regulation of metabolic flux," *Nature Reviews Bioengineering*, pp. 1–9, 2023.

[4] A. P. Darlington, A. A. Mannan, and D. G. Bates, "Natural host feedback simplifies the design of metabolic switches," in *2023 62nd IEEE Conference on Decision and Control (CDC)*, 2023, pp. 2693–2698.

[5] A. Mannan and D. Bates, "Designing an irreversible metabolic switch for scalable induction of microbial chemical production," *Nature Communications*, p. 3419, 2021.

[6] C. V. Dinh and K. L. J. Prather, "Development of an autonomous and bifunctional quorum-sensing circuit for metabolic flux control in engineered escherichia coli," *PNAS*, vol. 116, pp. 25 562–25 568, 2019.

[7] C. Ni, C. V. Dinh, and K. L. J. Prather, "Dynamic control of metabolism," *Annual Review of Chemical and Biomolecular Engineering*, pp. 1–23, 2021.

[8] Y. Qian, H. ho Huang, J. I. Jiménez, and D. D. Vecchio, "Resource competition shapes the response of genetic circuits," *ACS Synthetic Biology*, vol. 6, pp. 1263–1272, 7 2017.

[9] A. Darlington, J. Kim, J. Jiménez, and D. Bates, "Dynamic allocation of orthogonal ribosomes facilitates uncoupling of co-expressed genes," *Nature Communications*, vol. 9, 2018.

[10] A. Y. Weiße, D. A. Oyarzún, V. Danos, and P. S. Swain, "Mechanistic links between cellular trade-offs, gene expression, and growth," *Proceedings of the National Academy of Sciences*, vol. 112, pp. E1038–E1047, 2015.